American Mineralogist, Volume 84, pages 965–969, 1999

Location of interstitial Cr in mullite by incoherent channeling patterns from characteristic X-ray emission

C.J. ROSSOUW* AND P.R. MILLER

CSIRO Division of Manufacturing Science and Technology, Private Bag 33, Clayton South MDC, Australia 3169

ABSTRACT

The use of a direct crystallographic technique is reported for locating Cr atomic sites in a mullite containing 11.5 wt% Cr_2O_3 by monitoring variations in characteristic X-ray emission rates as a function of fast electron beam orientation. Systematic examination of two dimensional incoherent channeling patterns (ICP), formed from characteristic X-ray emissions from Al, Si, and Cr, and recorded near low index zone axis orientations, has enabled the preferred lattice position of Cr in mullite to be identified as the interstitial site 0, 0.25, 0. Although the method of atom location by channeling enhanced microanalysis (or ALCHEMI) generally has been applied in situations where introduced minority atom species are accommodated in substitutional atomic positions, this study illustrates the identification of an interstitial site of an introduced dopant species. This result does not coincide with that derived from X-ray Rietveld refinement. The ICP method is analytically robust and, unlike Rietveld refinement, does not require a highly accurate model of the host lattice framework and composition. ICP analysis therefore may be more appropriate for this particular application.

INTRODUCTION

Mullite belongs to the aluminum silicate group of minerals with the general formula $Al_{(4+2x)}Si_{(2-2x)}O_{(10-x)}$ (Cameron 1977). Although Burnham (1963) mentioned that, from a structural point of view, a complete solid solution can be expected in the compositional range between x = 0 (50 mol% Al_2O_3, or sillimanite) and x = 1 (100 mol% Al_2O_3, or iota-Al_2O_3), this has not been observed experimentally. Compounds of x = 0 composition with mullite-like structures are sillimanite and andalusite; both occur at elevated temperatures and pressures only. At a formation pressure of 1 atm, mullite is the only stable phase. Mullites generally have compositions between about x = 0.25 (stoichiometric or 3:2-mullite) and x = 0.4 (or 2:1 mullite). Syntheses using the sol-gel route below ~1000 °C (single phase or type I precursors, see Schneider et al. 1993) yield mullites with higher Al_2O_3 contents, up to x ≈ 0.6. Recently Fischer et al. (1994) described mullites with extremely high Al_2O_3 contents, corresponding to x = 0.9. In spite of earlier predictions (Saalfeld 1962; Perotta and Young 1974), it has not been possible as yet to synthesize the x = 1 compound (or iota-Al_2O_3) with the mullite or sillimanite structure. The [001] projection of the mullite structure is shown in Figure 1, and can be described by an orthorhombic cell consisting of chains of edge-sharing AlO_6 octahedra running along the *c* axis, with the point M1 chosen as the unit cell origin. These octahedral chains are cross-linked by $(Si,Al)O_4$ tetrahedral double chains (designated as T). The compositional change of mullite is the result of Al substitution for Si, which produces a composition related to the number of oxygen vacancies in the tetrahedral double chains that run along the *c* axis. Associated with these oxygen vacancies is the formation of a new tetrahedral site (designated as T*) that is cross-linked to two other T tetrahedra over a common oxygen atom (or tetrahedral triclusters).

Synthesis experiments on various mullites doped with transition metals were carried out by Schneider and coworkers (see Schneider et al. 1994 and references therein). The kind and amount of transition metal incorporated into the mullite structure depends on both the cation radius and valence, as well as the synthesis temperature and atmospheric environment. Mullite structures that include various additions of Ti_2O_3, TiO_2, V_2O_3, VO_2, Cr_2O_3, MnO, Mn_2O_3, FeO, Fe_2O_3, and CoO have been described. Highest degrees of accommodation within the crystal lattice have been observed for V_2O_3, Cr_2O_3, and Fe_2O_3, whereas only low or very low amounts of Mn_2O_3, TiO_2, and Ti_2O_3, and MnO, FeO and CoO, respectively, enter the mullite structure.

Rager et al. (1990) performed EPR studies on Cr-doped mullites, and found spectra consisting of two sharp signals near g_{eff} = 5 and a broad asymmetrical peak near g_{eff} = 2.2. The former was attributed to Cr in a strong crystal field with orthorhombic character. Referring to EPR data from sillimanite, Rager et al. (1990) correlated the EPR peaks near g_{eff} = 5 to the occurrence of Cr in slightly distorted regular octahedral M1 positions in mullite (the M1 position is chosen as the unit-cell origin). The broad EPR signal at g_{eff} = 2.2 was assigned to Cr cations most probably occurring in pairs, groups, or clusters in interstitial lattice sites. Rager et al. (1990) pointed out that Cr incorporation in regular M1 octahedra sites is preferred at low bulk Cr_2O_3 contents, whereas the signal assigned to interstitial Cr gradually becomes predominant at higher Cr_2O_3 contents (especially above 5 wt% Cr_2O_3; see Fig. 3 in Rager et al. 1990).

Due to the strong preference of Cr for octahedral coordination (Wells 1984), Rager et al. (1990) suggested that intersti-

* E-mail: rossouw@rivett.mst.csiro.au

0003-004X/99/0506–0965$05.00

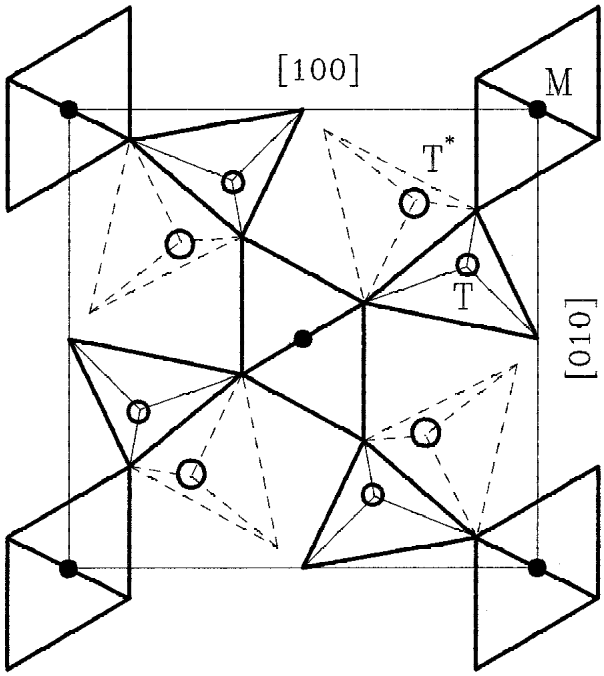

FIGURE 1. Projected [001] mullite structure showing M1, T, and T* sites, and oxygen tetrahedra and octahedra.

tial Cr cations are positioned at distorted octahedral environments. Starting from a crystallochemical approach, Rager et al. (1990) believed that possible interstitial sites occur near oxygen vacancies at 0.1, 0.25, 0 (designated as I1) or, alternatively, in the open structural channels running parallel to the *c*-axis at 0.2, 0.5, 0 (designated as I2). The occurrence of both regular octahedral M1 and interstitial Cr in mullite has been supported by optical absorption measurements (Ikeda et al. 1992), emission spectroscopy (Piriou et al. 1996), and EXAFS (Bauchspiess et al. 1996).

In this paper, a direct crystallographic technique is used for locating Cr atomic sites within the mullite lattice by monitoring variations in characteristic X-ray emission rates as a function of the orientation of a fast electron beam. This technique of atom location by channeling enhanced microanalysis (ALCHEMI) was described initially by Taftø and Spence (1983), and has been applied mostly to situations where introduced minority atom species are accommodated in substitutional atomic positions (Rossouw et al. 1996a, 1996b), although some studies have been performed for more complex situations where introduced species occupy interstitial positions (Krishnan et al. 1985). In this study, two-dimensional incoherent channeling patterns (ICP), formed from characteristic X-ray peaks of Al, Si, and Cr, are recorded near low index zone axis orientations.

Recent developments in the theory of ionization under dynamical electron diffraction conditions (Allen and Rossouw 1989, 1993; Josefsson et al. 1994) have shown the influence of dechanneling (forming a "kinematic" background contribution to ICP contrast) to be very important, whereas fine detail in the shape or delocalization of the ionization potential provides a relatively small effect. Dechanneling is critically dependent on the localized inelastic scattering potential V'(r) for thermal diffuse scattering (TDS) and, together with the elastic potential V(r), is used in conjunction with a simplified model for ionization (namely a thermally smeared delta-function; see Rossouw 1995) to predict contrast from various possible interstitial sites in various projections. These calculated channeling patterns are correlated with experiment to determine (from pattern recognition) the most likely set of lattice sites occupied by the introduced Cr atoms.

EXPERIMENTAL METHODS

Sample synthesis

The Cr_2O_3-doped mullite was produced from 52 wt% Al_2O_3 (VAW, 302), 38 wt% SiO_2 (Ventron, 88316), and 10 wt% Cr_2O_3 (Merck, 2483). The carefully admixed starting powders were uniaxially pressed to provide samples 20 mm in diameter and 5 mm in height. These discs were annealed in a laboratory furnace at 1650 °C for 12 h. After reaction sintering, the material consisted of mullite crystals up to 20 µm in size and a minor amount of a coexisting silicate glass. Microprobe analysis yielded a mullite composition (in wt%) of 60.0(4) Al_2O_3, 28.4(3) SiO_2, and 11.5(2) Cr_2O_3, which corresponds to a formula of $Al_{3.920}Cr_{0.505}Si_{1.575}O_{9.788}$.

ICP experiments

The disks of Cr_2O_3-doped mullite were cut to 3 mm and then ground to 0.2 mm in thickness prior to dimpling and ion-beam thinning procedures. These were mounted in a Gatan low-temperature double-tilt stage in a Philips CM30 analytical transmission electron microscope. An electron beam voltage of 201.5 keV was used, together with a temperature of 100 K during data acquisition to reduce TDS and to optimize channeling effects. A focussed probe with a 1.8 mrad total convergence angle and 0.4 µm diameter was aligned close to various zone axes on specimen areas up to 0.5 µm thick. Beam rocking and X-ray count acquisitions were controlled externally by computer, acquisition times being 1 s/pixel. The full X-ray spectrum was stored for each pixel, using an energy-dispersive X-ray (EDX) detector with a take-off angle of 20°.

Background-corrected characteristic X-ray counts subsequently were displayed as 79 × 58 pixel maps, corresponding to ICP with an angular range of 95 mrad along the *x*-axis. Backscattered electron (BSE) channeling maps were used primarily for setting up experimental conditions prior to allocating control to the computer, BSE contrast being closely related to contrast formed from X-ray emission in ICP (Rossouw et al. 1994).

ICP contrast

The undoped mullite structural data, atomic positions, and distributions as well as Debye-Waller factors were taken from Angel and Prewitt (1986), conforming to the orthorhombic Pbam (D92h) structure (no. 55 in the *International Tables for X-ray Crystallography*, Ibers and Hamilton 1974). Lattice constants used for the Cr_2O_3-doped structure were a = 7.5674 Å, b = 7.7089 Å, and c = 2.901 Å, respectively, as measured by Rager et al. (1990). ICP from M1, T, and T* sites, as well as ICP for interstitial positions, were calculated using a thermally smeared δ-function for an undoped mullite crystal assumed to be 0.4 µm thick. ICP for Al and Si atoms distributed over these

sites were calculated from the formulae Al = 0.42 M1 + 0.47 T + 0.11 T*, and Si = 0.81 T + 0.19 T*, using the structural data of undoped mullite (such a representation is necessary because each calculated ICP is normalized to one atom per site). Using Doyle and Turner (1968) X-ray scattering factors, converted via the Mott formula to electron-scattering factors, the mean inner potential V_o is calculated to be 15.15 volts.

Calculated ICP were generated by a rastered scan of test positions within the projected unit cell for both the [100] and [010] zone axis projections and, from changes in contrast as a function of atomic position within the unit cell, a resolution of about 0.3 Å appears to be possible. The best match with the experimental Cr ICP occurs when the site 0, 0.25, 0 is occupied, this position being designated hereafter as the interstitial site I.

[100] zone

The projected [100] structure in Figure 2 (2 × 2 unit cells) shows that the M1 sites form a rectangular lattice, whereas T and T* sites form well-defined {001} planes. The interstitial site I forms a lattice similar to M1 but displaced by 0, 0.25, 0. Experimental ICP formed from characteristic Al, Si, and Cr X-rays are shown in Figure 3. Here the reciprocal space scan pattern is aligned such that g_x = 020 and g_y = 001: Vertical Brillouin zone (BZ) boundaries correspond to exact Bragg orientation of n g_x beams, and similarly horizontal lines of contrast indicate loci of exact Bragg orientation for n g_y beams. A horizontal scan from the center to the edge of the ICP crosses approximately eleven higher order 020 BZ boundaries. The first pair of numbers in each caption gives the maximum and minimum X-ray counts or, for the case of calculated patterns, the maximum and minimum in the dynamical enhancement factor. The second pair of numbers give contrast settings with 16 gray levels on a logarithmic scale between max and min, expressed as a percentage of (max - min), the first number representing the white level and the second number the black level.

Calculated ICP formed by characteristic X-rays from atoms occupying M1, T, and T* site responses are shown in Figure 4, together with calculated ICP for Al and Si. In detail, the M1 response close to the zone axis orientation has vertical excess bands between the second and third BZ boundary along g_x and within the first order BZ along g_y. Horizontal excess bands occur in the region bounded by the first and second order g_y BZ and the first order g_x BZ. These enhanced regions in reciprocal space change to deficit bands for emission from the T* site, whereas the T site displays enhanced emission in the center of the pattern within second order g_x and first order g_y BZ

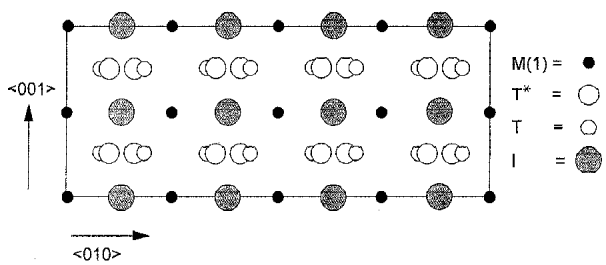

FIGURE 2. Projected [100] mullite structure showing M1, T, and T* sites, together with interstitial site I.

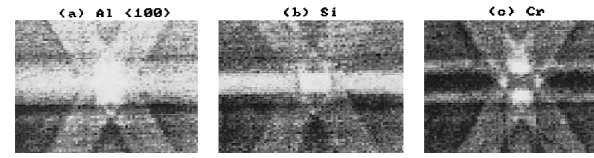

FIGURE 3. Experimental [100] ICP showing **(a)** Al with counts between 1681 and 908 (max, min) contrast settings of 90 and 15% (white, black), hereafter referred to as (max,min and white%,black%); **(b)** Si counts (769,324 and 90,15); and **(c)** Cr counts (633,186 and 80,10).

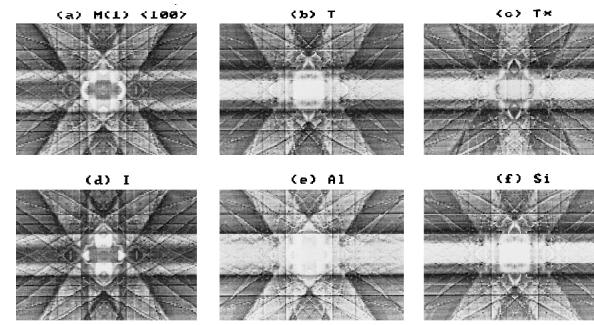

FIGURE 4. Calculated [100] ICP for sites **(a)** M1 (3.3,0.37 and 90,5), **(b)** T (2.3,0.43 and 90,5), and **(c)** T* (2.2,0.42 and 90,5), together with responses for interstitial sites I in **(d)** (3.4,0.44 and 90,5). Reconstructed responses in **(e)** for Al (2.1,0.42 and 90,5), and in **(f)** for Si (2.1,0.44 and 90,5).

boundaries. The ICP in Figure 4d, formed by characteristic X-rays from atoms occupying site I, has the pair of horizontal bands between the second and third order g_y BZ boundaries (similar to the M1 site pattern), but is enhanced further within these bands within the first order g_x BZ. A pair of "arrowheads" occurs within the first order g_y BZ boundaries between the third and fourth order g_x BZ boundaries.

Taking a wider angle view, M1 and the interstitial site are characterized by a pair of horizontal excess bands that lie between the first and second order g_y BZ boundaries, whereas one excess band occurs from T and T* sites within the first order g_y BZ. Vertical excess bands occur within second order g_x boundaries, except for T sites, which are characterized by vertical deficit bands away from the zone axis orientation. Enhancement occurs on all sites within the crossed g_{041} BZ boundaries, except for T* sites, which display overall deficit scattering within these bands.

Calculated Al and Si responses show geometry similar to experiment, detailed correlation being better for the Si responses. For Al, however, the calculated central rectangular minimum is not present in experiment, possibly due to a smaller occupancy of the M1 site by Al. Correlation of experiment in Figure 3c with calculation in Figure 4d indicates that Cr does not favor substitutional sites M1, T, or T*, but substantially occupies the interstitial site I.

[010] zone

The projected structure (2 × 2 unit cells) in Figure 5 shows M1 sites retain a rectangular lattice similar to the [100] projection, but that interstitial sites I now project onto this site. Once

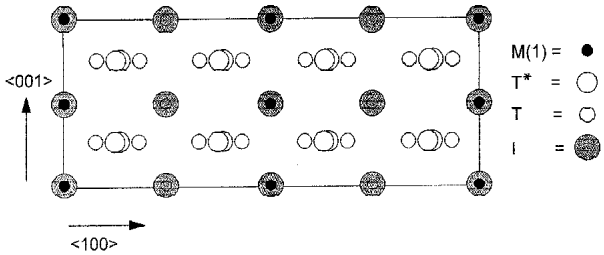

FIGURE 5. Projected [010] mullite structure showing M1, T, T* and I sites.

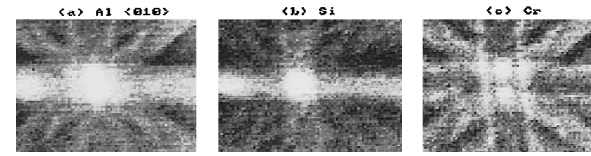

FIGURE 6. Experimental [010] ICP showing **(a)** Al (1441,705 and 90,15), **(b)** Si (606,235 and 90,15), and **(c)** Cr (433,152 and 80,10).

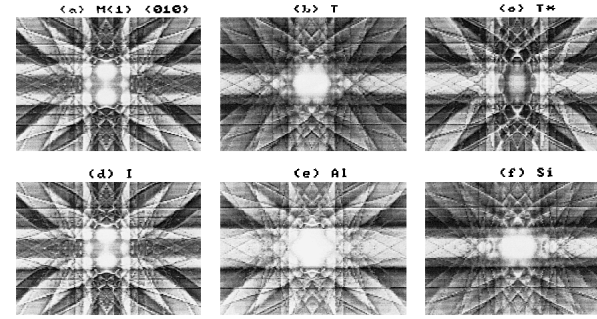

FIGURE 7. Calculated [010] ICP for sites **(a)** M1 (2.8,0.4 and 90,5), **(b)** T (2.9,0.42 and 90,5), and **(c)** T* (2.6,0.4 and 90,5), together with responses for interstitial sites I in **(d)** (2.8,0.4 and 90,5). Reconstructed responses are shown in **(e)** for Al (2.1,0.45 and 90,5) and in **(f)** for Si (2.6,0.45 and 90,5).

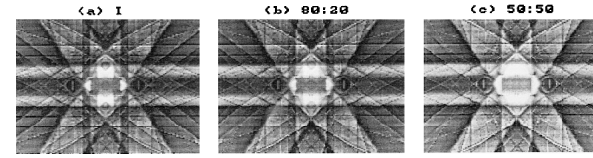

FIGURE 8. Calculated [100] ICP for the interstitial site I, showing the pattern expected from (a) 100% occupancy of I sites (3.4,0.44 and 90,5), (b) an occupancy ratio of 80:20 of I:M1 sites (2.1,0.44 and 90,5), and (c) a ratio of 50:50 of I:M1 sites (2.5,0.41 and 90,5).

more, the T and T* sites form well-defined {001} planes, with T* coming closer together whereas the spacing of T sites remains similar to the [100] projection in Figure 2.

Experimental [010] ICP are shown in Figure 6, and calculated ICP formed by characteristic X-rays from atoms occupying M1, T, T*, and I sites in Figure 7, together with the overall responses from Al and Si atoms. The scan directions are aligned such that $g_x = 200$ and $g_y = 001$. For the M1 site, vertical excess bands occur between the horizontal second and third BZ boundary along g_x, and horizontal excess bands between the first and second order g_y BZ. Where these excess bands intersect, stronger enhancement takes place. Enhanced lobes also occur within the horizontal excess bands and within the first order g_x BZ boundaries. For the T site, an excess horizontal band occurs within first order g_y BZ boundaries, and an excess vertical band within the second order g_x BZ. A similar horizontal band occurs for the T* site, but a pair of excess vertical bands now exists between third and 4th order g_x BZ boundaries. In this projection, ICP contrast from interstitial site I is identical to ICP contrast from M1 sites, these being indistinguishable in projection along [010].

Calculated Al and Si ICP in Figure 7 show good agreement with experiment in Figure 6, although some distortion of experimental ICP is evident due to beam shift and local crystal bending. The experimental Cr pattern is remarkably similar to that expected from M1 or I sites. Since correlation between experimental and calculated ICP for the [100] zone excludes the M1 position for Cr, it is clear that interstitial position I is the preferred lattice site for incorporation of Cr within the mullite crystal.

DISCUSSION

Variations in characteristic X-ray emission rates under systematically scanned, strong zone axis diffraction conditions have been used to identify the Cr site within a mullite crystal lattice. This has been achieved by the inherent symmetries and associated pattern recognition of two-dimensional ICP from the constituent atoms. Correlation between experiment and calculated ICP for Si and Al X-rays shows good evidence that Si is restricted to T and T* positions within the lattice. Although Al occupies M1, T, and T* positions, occupancies derived by Angel and Prewitt (1986) appear to overestimate the occupancy of M1 sites by Al in our particular mullite specimen.

Comparison of experiment with calculated ICP shows that Cr occupies neither the regular lattice sites nor the interstitial sites suggested by Rager et al. (1990) (i.e., 0.1, 0.25, 0 and 0.2, 0.5, 0, designated as I1 and I2, respectively). According to the present systematic ICP analysis, most of the Cr occupies an interstitial position I at 0, 0.25, 0 although, as shown in Figure 8, some minor amount of Cr may be situated at M1 sites. The possibility of large amounts of Cr at M1 sites (50% or more) is discounted, since the calculated ICP is then significantly different from experiment. In fact, it should be pointed out that the clear contrast in experimental ICP indicates that Cr cations occur in well-defined interstitial positions, and are not distributed randomly along structural channels within the mullite lattice. Calculations for a variety of idealized mullite structures (with composition parameter x in the range 0.2–0.6) showed that, although the scattering potential of difference reflections such as {020}, {200} and {001} is reasonably sensitive to x, overall ICP contrast is not. Thus the ICP "fingerprint" from different sites is largely defined by the overall structural framework, and (unlike scattering potentials for specific beams) is insensitive to the fine structural detail and the x-dependence of host atom site occupancies in mullite.

X-ray Rietveld structural refinements on Cr_2O_3-doped mul-

lite (R.X. Fischer, unpublished data, 1998) lead to the conclusion that Cr in the mullite lattice is located on the M1 site rather than the I site as determined by ICP analysis. Indeed, Rietveld refinements conducted in our laboratories on the same sample as was used for the ICP experiments (D. Hay, personal communication, 1997) lead to a similar result, assuming the Angel and Prewitt (1986) structure. However, Rietveld refinement requires, as a starting point, a model that is a reasonable approximation to the actual crystal structure (Bish and Post 1989). The ICP method is less sensitive to small variations in crystal structure, depending on a projected two-dimensional structure for each pattern rather than the full three-dimensional structure. Here. two components of the full three dimensional Cr site co-ordinates are retrieved from a single zone axis pattern, and orthogonal [100] and [010] projections were used to obtain a complete co-ordinate set. As previously noted, detailed analysis of contrast in the ICP suggests that significant differences exist between the actual crystal structure of Cr_2O_3-doped mullite and the modeled structure. The detailed defect structure of mullite has been investigated by Welberry and Withers (1990) and Butler and Welberry (1994), using analysis of the diffuse scatter of X-rays over all angles. The degree of short range order of vacant oxygen sites may lead to an averaged structure that is not representative of the detailed local structure and, in particular, the local environment of the introduced Cr cations may be associated with surrounding defects in the oxygen sublattice. Another possible source of the discrepancy between Rietveld and ICP results is the fact that whereas powder XRD diffraction methods sample many crystallites, the ICP method is specific for a particular crystallite (10–20 μm in size). The examination of many individual crystallites by ICP has not yet taken place, and the possibility of more than one mode of Cr incorporation within the lattice has not been precluded. Thus, although we have shown that the ICP method may be used to obtain the structural environment of Cr directly in mullite, reasons for the discrepancy with results obtained from Rietveld refinement are not yet clear. Possibilities include anomalies introduced by sampling of individual grains by ICP rather than a large number by Rietveld, or anomalies due to greater sensitivity of Rietveld to the precise average structure assumed for the lattice compared with ICP analysis. However, on the proviso that the mode of Cr incorporation is the same in the two grains examined, the ICP result is unambiguous, i.e., Cr has been found to occupy the interstitial site I = 0, 0.25, 0, rather than the M1 site as derived from Rietveld refinement.

ACKNOWLEDGMENTS

We acknowledge the work of David Hay in our laboratories in collection of X-ray data and for Rietveld refinement on the particular mullite investigated in this paper. We also acknowledge discussions with Hartmut Schneider of the Institute for Materials Research (German Aerospace Research Establishment, Cologne, Germany) on this paper, and for provision of the original mullite sample.

REFERENCES CITED

Allen, L.J. and Rossouw, C.J. (1989) Effects of thermal scattering and surface tilt on diffraction and channeling of fast electrons in CdTe. Physical Review B, 39, 8313–8321.

—— (1993) Delocalization in electron impact ionization in a crystalline environment. Physical Review B, 47, 2446–2452.

Angel, R.J. and Prewitt, C.T. (1986) Crystal structure of Mullite: A re-examination of the average structure. American Mineralogist, 71, 1476–1482.

Bauchspiess, K.R., Schneider, H., and Kulikov, A. (1996) EXAFS studies of Cr-doped Mullite. Journal of the European Ceramic Society, 16, 203–209.

Bish, D.L. and Post, J.E. (1989) Rietveld refinement of crystal structures using powder X-ray diffraction data. In Mineralological Society of America Reviews in Mineralogy, 20, 277–308.

Burnham, C.W. (1963) Refinement of the crystal structure of sillimanite. Zeischrift für Kristallographie, 115, 127–148.

Butler, B.D. and Welberry, T.R. (1994) Analysis of diffuse scatter from the Mineral Mullite. Joural of Appllied Crystallography, 27, 742–754.

Cameron, W.E. (1977) Mullite: A substituted alumina. American Mineralogist, 62, 747–755.

Doyle, P.A. and Turner, P.S. (1968) Relativistic Hartree-Fock X-ray and electron scattering factors. Acta Crystallographica, A24, 390–397.

Fischer, R.X., Schneider, H., and Voll, D. (1994) Formation of aluminium rich 9:1 mullite and its transformation to low alumina mullite upon heating. Journal of the European Ceramic Society, 16, 109–113.

Ibers, J.A. and Hamilton, W.C., Eds. (1974) International Tables for X-ray Crystallography, Vol. IV, Kynoch, Birmingham, U.K.

Ikeda, K., Schneider, H., Akasaka, M., and Rager, H. (1992) Crystal-field spectroscopic study of Cr-doped mullite. American Mineralogist, 77, 251–257.

Josefsson, T.W., Allen, L.J., Miller, P.R., and Rossouw, C.J. (1994) K-shell ionization under zone axis electron diffraction conditions. Physical Review B, 50, 6673–6684.

Krishnan, K.M., Rez, P., and Thomas, G. (1985) Crystallographic site-occupancy refinements in thin-film oxides by channeling-enhanced microanalysis. Acta Crystallographica B, 41, 396–405.

Perotta, A.J. and Young, J.E. (1974) Silica-free phases with mullite-type structures. Journal of the American Ceramic Society, 57, 405–407.

Piriou, B., Rager, H., and Schneider, H. (1996) Time-resolved Fluorescence Spectroscopy of Cr^{3+} in Mullite. Journal of the European Ceramic Society, 16, 195–201.

Rager, H., Schneider, H., and Graetsch, H. (1990) Chromium incorporation in mullite. American Mineralogist, 75, 392–397.

Rossouw, C.J. (1995) Incoherent contrast under dynamical diffraction conditions. Ultramicroscopy, 58, 211–222.

Rossouw, C.J., Forwood, C.T., Gibson, M.A., and Miller, P.R. (1996a) Statistical ALCHEMI: General formulation and method with application to TiAl ternary alloys. Philosophical Magazine A, 74, 57–76.

—— (1996b) Zone axis CBED and ALCHEMI analysis of TiAl alloys with ternary additions. Philosophical Magazine A, 74, 77–102.

Rossouw, C.J., Miller, P.R., Josefsson, T.W., and Allen, L.J. (1994) Zone axis backscattered electron contrast for fast electrons. Philosophical Magazine A, 70, 985–998.

Saalfeld, H. (1962) A modification of Al_2O_3 with the sillimanite structure. In: transactions VIIIth International Ceramic Congress, Copenhagen, p. 71–74.

Schneider, H., Saruhan, B., Voll, D., Merwin, L., and Sebald, A. (1993) Mullite precursor phases. Journal of the European Ceramic Society, 11, 87–94.

Schneider, H., Rodewald, K., and Eberhard, E. (1994) Thermal expansion discontinuities of mullite. Journal of the American Ceramic Society, 76, 2896–2898.

Taftø, J. and Spence, J.C.H. (1983) Crystal site location of iron and trace elements in a magnesium-iron olivine by a new crystallographic technique. Science, 218, 49–51.

Wells, A.F. (1984) Structural Inorganic Chemistry, 5th edition. Clarendon Press, Oxford.

Welberry, T.R. and Withers, R.L. (1990) An optical transform and Monte Carlo study of the diffuse X-ray scattering in mullite, $Al_2(Al_{2+2x}Si_{2-2x})O_{10-x}$. Physics and Chemistry of Minerals, 17, 117–124.

MANUSCRIPT RECEIVED JUNE 18, 1998
MANUSCRIPT ACCEPTED DECEMBER 14, 1998
PAPER HANDLED BY ADRIAN J. BREARLEY